---

**Article:**
Alsebaie, D.M. orcid.org/0009-0003-0398-2062 and Morley, N.A. orcid.org/0000-0002-7284-7978 (2025) Impact of increasing aluminium content on the magnetic, electrical, and structural properties of FeCoNiMnAl thin films. IEEE Transactions on Magnetics. ISSN 0018-9464

https://doi.org/10.1109/tmag.2025.3566139

---

# Impact of Increasing Aluminium Content on the Magnetic, Electrical, and Structural Properties of FeCoNiMnAl Thin Films

D.M. Alsebaie [1,2,*] and N. A. Morley [1]

[1] School of Chemical, Materials and Biological Engineering, University of Sheffield, S13JD, UK

[2] Physics Department, King Abdulaziz University, Jeddah, Saudi Arabia

[*] Corresponding author: Dalsebaie1@sheffield.ac.uk

This paper studies the magnetic and electrical properties of adding Al and Mn to the ternary FeCoNi alloy. FeCoNi has soft magnetic properties; however, due to Co and Ni being classed as critical materials, reducing their content in the films while enhancing the magnetic and electrical properties is important for future applications. The magnetic thin films were prepared using DC sputtering, with all the films having an uniform thickness of 100 nm. The crystal structure of the films was analysed using XRD, which revealed a change from FCC for the FeCoNi film to BCC for the FeCoNiMnAl films. The composition of the films was determined using X-ray Photoelectron Spectroscopy (XPS). It was found that adding Mn to FeCoNi did not result in any noticeable magnetic improvement, but a change in morphology within the films from polycrystalline to amorphous. However, when both Al and Mn were added to FeCoNi, the coercivity and remanence decreased as the Al content increased, while the films now had a nanocrystalline BCC morphology. Additionally, the $Fe_{1.4}Co_{1.2}Ni_{1.1}MnAl_2$ composition showed lower coercivity and remanence compared to FeCoNi. The saturation magnetization exhibited a significant decrease as the amount of Al and Mn in the films increased. While the electrical resistivity increased with the addition of Al and Mn. Finally, $Fe_{1.4}Co_{1.1}Ni_{1.1}MnAl_{1.3}$ appears to be a promising candidate for soft magnetic applications due to its reduced cost compared to FeCoNi and its improved resistivity compared to permalloy.

*Index Terms*— Soft magnetic materials, FeCoNi, magnetic properties, electrical properties.

## I. Introduction

The prospective uses for soft, high-moment magnetic films are within storage devices, high frequency applications and sensors due to their considerable saturation magnetisation (>800 kA/m) and minimal coercivity (<0.2 A/m) [1]. The growing interest in miniaturising device size has driven the investigation into producing and characterising new soft magnetic films [2]. Permalloy, which is based on $Fe_{20}Ni_{80}$, is a well-known soft magnetic film characterised by its high relative permeability (100000), low coercivity ($H_c$= 0.2 A/m), and moderate saturation magnetisation, ($M_s$ = 795 kA/m) [3, 4], but the higher saturation magnetisation in Ni-Fe alloys is limited to the equiatomic composition, which also have a large coercive field. Among all the Fe group alloys, binary Fe-Co alloys demonstrate the highest saturation magnetisation, measuring approximately 1909 kA/m. However, the use of Fe-Co alloys in magnetic industries is restricted due to their high coercivity (150 A/m) [5, 6], brittleness, and inadequate corrosion resistance [3, 7]. Additionally, it has been observed that both Fe-Co and Fe-Ni alloys do not exhibit a significant level of electrical resistivity, a crucial factor in mitigating the losses caused by eddy currents. Consequently, there exists a significant inclination to explore ternary Fe-Co-Ni alloys due to their exceptional magnetic characteristics in conjunction with anti-corrosive attributes [4, 8]. It has been observed that ternary Fe-Co-Ni alloys exhibit a notable saturation magnetisation ($M_s$ = 1100 kA/m) in conjunction with a reduced coercivity (400 A/m) in comparison to conventional permalloy [4]. Furthermore, it has been observed that electrodeposited Fe-Co-Ni films demonstrate significant magnetoresistance [9]. The significance of controlling the chemical composition is apparent when examining the ternary phase diagram of Fe-Co-Ni with respect to composition and temperature, as well as the magnetic phase diagram.

Even small alterations in chemical composition can result in substantial modifications to the structure, microstructure, and magnetic characteristics [8]. Fe-Co-Ni films have garnered growing attention in recent years due to their classification as medium entropy alloys [10]. These alloys, when combined with appropriate alloying additives such as aluminium (Al), manganese (Mn), boron (B), and chromium (Cr), demonstrate promising exceptional mechanical, corrosive, and magnetic qualities [4]. These 4 or more element alloys are often known as high entropy alloys (HEAs),

and work exploring their soft magnetic properties is ongoing. Previous work studying CoFeNiCr-X, where X = Cu, Al [11-13], found that the addition of Cr strongly reduced the magnetization and Curie Temperature, so they were not suitable for soft magnetic applications. Therefore further work investigating CoFeNiMn-X based HEAs is looking more promising, as the Mn does not cause the large drop in Curie Temperature that the addition of Cr does.

Adding equal percentages of Al and Mn to FeCoNi in a bulk alloy alters the crystal structure from a face centred cubic (FCC) to body centred cubic (BCC) and enhances the soft magnetic properties. Bazioti et al. investigated $FeCoNi(AlMn)_x$ high-entropy alloy (HEA) samples prepared through laser metal deposition (LMD). X-ray diffraction (XRD) analysis demonstrated that increasing Al and Mn content progressively shifted the crystal structure from an FCC phase to a BCC phase. Additionally, the study found that the soft magnetic properties improved as the Al and Mn concentrations increased in equal proportions [14]. Other work on bulk CoFeMnAl [15] , found an increase in the magnetization, with increasing the Al concentration, due to the Al stabilizing a BCC phase within the alloys, the disadvantage was that the coercive field was relatively high as well.
The phases present in a HEA strongly depend upon the enthalpy of mixing of each element and the valence electron concentration (VEC). Figure 1 gives the enthalpy of mixing for the five elements studied within the films studied in this paper. It is observed that Al has high negative enthalpy of mixing with Co, Ni and Mn, which means it is most likely to strongly pair with these elements, plus a reasonable negative value for Fe. This suggests that a single phase is likely to form, rather than mixed phases, due to no pair having a much larger mixing value compared to the others.

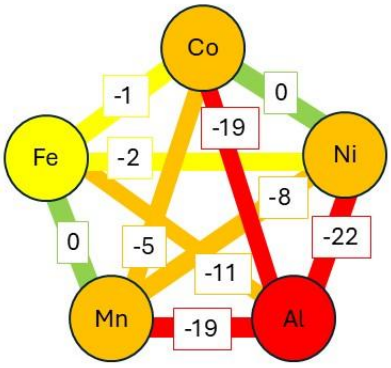


Figure 1 Enthalpy of mixing values for the five elements studied within this paper. The unit on the enthalpy of mixing values is kJ/mol.

The transition from the FCC to the BCC phase is due to the VEC value for each of the compositions studied. It has been shown that for alloys with VEC > 8, the phase will be FCC, for 8 > VEC > 6.87 the alloy will have mixed FCC and BCC phases, and for 6.7 > VEC, the alloy should contain just BCC[16]. For equimolar CoFeNi, the VEC is 9, and therefore should be FCC, which has been confirmed by experiments. While for equimolar CoFeNiMn, the VEC is 8.5 and again should be FCC. For equimolar CoFeNiMnAl, the VEC is 7.4 and therefore a mixed FCC+BCC phase should be present. It is the addition of the Al that drives the BCC, as it reduces the VEC. Further previous work has found [15], that the BCC phase in HEAs has a higher saturation magnetization than the FCC phase, so the addition of the non-magnetic Al can help increase the saturation magnetization, by the formation of the BCC phase.

The majority of the research on HEAs has been carried out in bulk samples, while an increasing number of soft magnetic applications require thin films. Thus in this paper, we study how the addition of Al to CoFeNi-Mn films

changes the morphology, magnetic and electrical properties, to determine whether it has the same structure changes as bulk samples, and if the magnetic and electrical properties are competitive for applications.

## II. Experimental Work

In this paper, five samples were prepared via DC sputtering, using a 3-gun system to change the composition. Subsequently, their composition, crystal structure, electric and magnetic properties were measured. The DC sputtering technique was utilised to deposit FeCoNi, FeCoNiMn and FeCoNiMn$Al_x$ thin films onto Si (100) substrates. Before deposition, the 10 mm × 10 mm substrates were cleaned in an ultrasonic bath using acetone and isopropanol (IPA) for 10 minutes. Three targets were used within the system: FeCoNi with a composition of 33.3 at%. for each element and a purity of 99.9 %, Mn and Al each with a purity of 99.999 %. For the films studied, the film thickness was 100 nm, while the composition of the films was varied. This was done by changing the power of the Al gun, and growth time. The FeCoNiMnAl thin films were deposited with sputtering powers: $P_{FeCoNi}$ =70 W, $P_{Mn}$ = 35W, and $P_{Al}$ = 30, 60, and 90 W, and at a chamber pressure ($P_{Ar}$) of 0.7 Pa for different deposition times for each sample to ensure the films were all 100 nm thick. A low-field magneto-optical Kerr effect (LMOKE) magnetometer was used to assess the magnetic characteristics of the films in longitudinal mode. The DC magnetic field was strong enough to saturate the films with a maximum field value of 54 kA/m. The normalised magnetization hysteresis loops were measured by varying the direction of the applied magnetic field with respect to a single edge. The film was positioned at an angle of 0°, then the magnetic hysteresis loop was measured in the range from 0° to 180°. This enabled the determination of the in-plane magnetic anisotropy caused by growth parameters. The anisotropy field ($H_k$) was measured at $M/M_s$=1. The structure of the films was examined using X-ray diffraction (XRD) measurements conducted on a Bruker D2 phaser equipped with a Cu $K_{\alpha 1}$ (wavelength = 1.54184 Å) source and with an operational voltage of 40 kV and a current of 40 mA. θ/2θ measurements were conducted within a range of 40° to 50° to investigate the films' structure only, hence avoiding the Si substrate's large peaks at about 65°. Moreover, X-ray Photoelectron Spectroscopy (XPS) was used to identify the film's composition. The saturation magnetisation ($M_s$) was measured on a Superconducting Quantum Interference Device (SQUID). The hysteresis loops, also known as M-H loops, were measured at a temperature of 300 K and a magnetic field ranging from 800 kA/m to -800 kA/m. Furthermore, the electrical resistance was quantified using the four probe techniques, achieving an accuracy of 100 μΩ.

## III. Result and discussion

### *A. XRD result & XPS measurements*

Figure 2(a) shows the XPS spectrum for Al(2p) peaks for the different FeCoNiMnAl films. It clearly shows that the Al peak increases as its concentration increases from 11 to 29 at % in the films. Also, Table 1 shows the percentage of each element in the films, which was calculated using the CasaXPS software. Figure 2(b) shows the continued increase in the aluminium percentage as the aluminium target power was increased from 30, to 90 W, while the FeCoNi and Mn power were fixed at 70 and 35 W respectively. Figure 2(b) also, demonstrates a linear relationship between

the Al composition and Al sputtering power. Consequently, the aluminium composition can be controlled, while keeping all other fabrication settings constant.

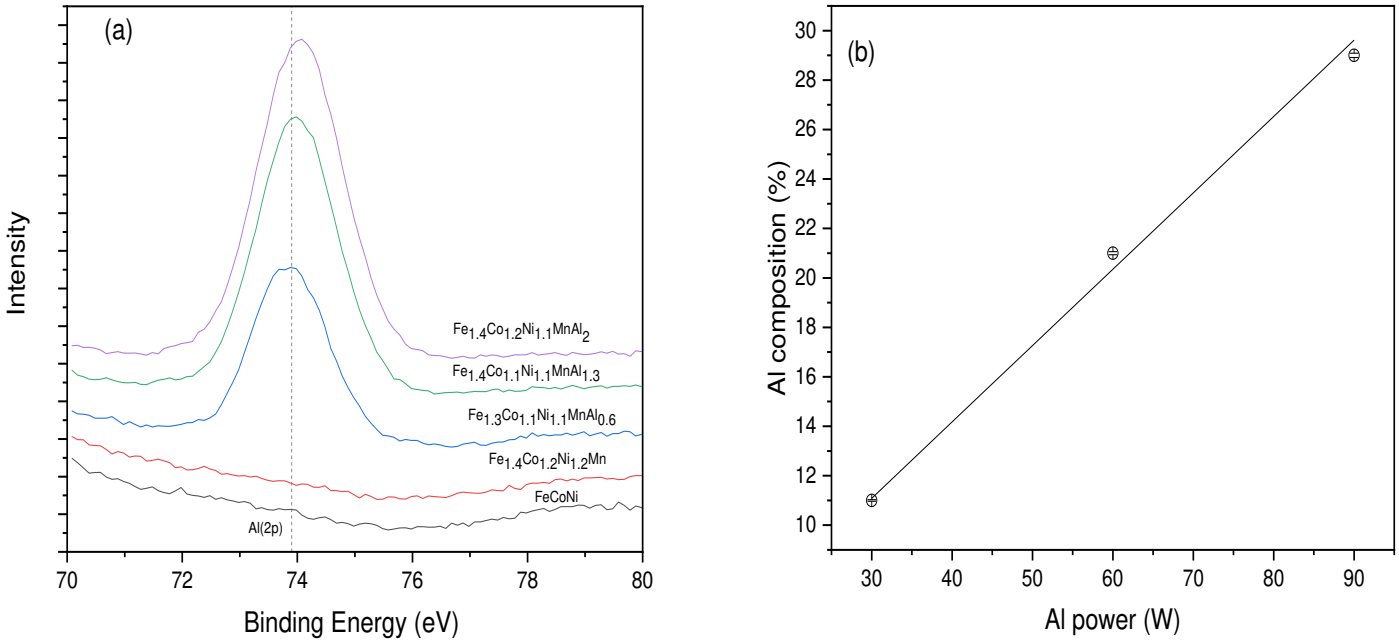


Figure 2. (a) XPS spectra for the Al(2p) for the FeCoNiMnAl. (b) Al composition as a function of Al sputtering power in the same conditions.

Table 1 The XPS result of the films composition, calculated VEC lattice constants and grain size from XRD peak.

| Film composition | Al power (W) | Ni (at%) | Co (at%) | Fe (at%) | Mn (at%) | Al (at%) | Lattice constant (Å) | Grain size (Å) | VEC |
|---|---|---|---|---|---|---|---|---|---|
| $FeCoNi_{(70W)}$ | 0 | 33 ± 2 | 32 ± 2 | 35 ± 2 | 0 | 0 | 3.55 ± 0.01 | 220 ± 5 | 8.98 |
| $FeCoNi_{(70W)}Mn_{(35W)}$ | 0 | 29 ± 2 | 26 ± 2 | 25 ± 2 | 20 ± 2 | 0 | - | - | 8.64 |
| $FeCoNi_{(70W)}Mn_{(35W)}Al_{(x)}$ | 30 | 26 ± 2 | 22 ± 2 | 21 ± 2 | 20 ± 2 | 11 ± 2 | 2.86 ± 0.01 | 204 ± 5 | 7.99 |
| $FeCoNi_{(70W)}Mn_{(35W)}Al_{(x)}$ | 60 | 24 ± 2 | 19 ± 2 | 19 ± 2 | 17 ± 2 | 21 ± 2 | 2.87 ± 0.01 | 259 ± 5 | 7.45 |
| $FeCoNi_{(70W)}Mn_{(35W)}Al_{(x)}$ | 90 | 21 ± 2 | 18 ± 2 | 17 ± 2 | 15 ± 2 | 29 ± 2 | 2.87 ± 0.01 | 285 ± 5 | 7 |

Figure 3 shows the X-ray diffraction (XRD) patterns for the FeCoNiMnAl films, which were used to determine whether the films were fully crystalline or amorphous. The bottom spectrum is for the Si substrate and shows a series of peaks associated with its single crystal structure. For the FeCoNi film XRD pattern, a single broad peak at about 44° is observed, which is associated with the (111) direction for Face centred cubic (FCC) [17, 18]. No other FCC peaks were observed, suggesting that the FeCoNi film had columnar growth in the (111) direction. The film becomes amorphous for the sample in which Mn is added to FeCoNi ($Fe_{1.4}Co_{1.2}Ni_{1.2}Mn$), as only the Si substrate peaks are

observed and can be fitted to (Figure 3b). Adding Aluminium to the FeCoNiMn films by different concentrations 0.6, 1.3 and 2 makes the films polycrystalline with Body centred cubic (BCC) as they shows a broader peak at about 44.5°, associated with the BCC (110) direction, compared to the Si substrate, which becomes bigger as the Al concentration increases [14, 18]. The fitting of the two peaks is shown in Figure 3b, where it is clear that the BCC peak is much broader that the sharp Si peak. No other BCC peaks are observed, which is expected as Fe-Co based alloys grown with columnar growth in the (110) direction on silicon substrates [14].

In HEAs, where 4 or more elements are mixed together in composition ranges from 15% to 35%, due to the high enthalpy of mixing between these elements, often single phases such as FCC and BCC form in these alloys. A simple way to predict the phases present is to use the valence electron concentration (VEC)[16]. It has been shown that for alloys with VEC > 8, the phase will be FCC, for 8 > VEC > 6.87 the alloy will have mixed FCC and BCC phases, and for 6.7 > VEC, the alloy should contain just BCC. The VEC for each of the compositions were calculated and are given in Table 1. It is observed at for the FeCoNi film, the VEC is 8.98, which is predicted to be FCC, and this is observed in the XRD pattern. The addition of Mn reduces the VEC, but it is still solidly within the FCC region, this is not observed within the film, due to the Mn causing the morphology to change to amorphous. The further additions of Al to the FeCoNiMn reduces the VEC to below 8, so into the mixed FCC and BCC region. This is observed in the XRD patterns, where a broad BCC peak starts to appear with the Al addition (Figure 3b). The FCC phase is not observed within these films, but this could be due to the Mn causing it to be amorphous, as observed in the FeCoNiMn film, so only the BCC phase is observed.

Moreover, the lattice constant and grain size for the films were calculated using Bragg's law and the Scherrer equation respectively and are presented in Table 1. These values were determined using Fityk software to fit the peaks for films containing Al concentrations of 0.6, 1.3, and 2. The lattice constants values are similar with the findings of Li et al.[17], with an increase in the BCC lattice constant as the Al is added. The grain sizes are all between 20-30 nm for the polycrystalline films, suggesting that the addition of Al hasn't strongly affected the grain growth.

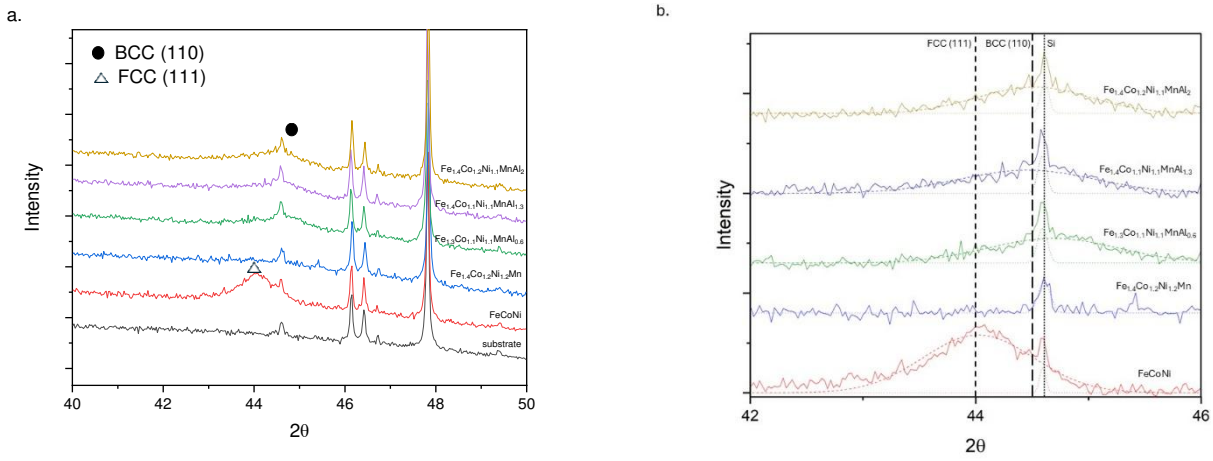


Figure 3a. X-ray diffraction (XRD) measurements for FeCoNiMnAl films. 3b. Focused region for the FeCoNiMnAl films, where the solid lines are the measured data, and the dashed and dotted lines are for the fits to the data. The main phases are given by the vertical dashed lines.

### *B. Magnetic properties*

Figure 4 shows the changes in the normalised magnetic hysteresis loops of the FeCoNiMnAl films with the addition of Mn and Al, as depicted in figures 4 (a-e). Figure 4(a) for the FeCoNi film, displays the approximate optimum easy and hard axes for an ideal magnetic film, which obeys the Stoner-Wohlfarth model. Figure 4(f) gives the coercive field and remanence values for all the films, measured from the hard axis. For the first two compositions (with Al = 0), the FeCoNi film exhibits a low coercive field and remanence. However, upon the addition of Mn, forming

$Fe_{1.4}Co_{1.2}Ni_{1.2}Mn$, the remanence jumps to its highest value, approximately 0.44, and the coercive field increases to 2.3 kA/m. In the remaining three samples, with Al concentrations of 0.6, 1.3, and 2, increasing the Al content causes the films to become magnetically softer, as indicated by a reduction in the coercive field and remanence. The $Fe_{1.4}Co_{1.2}Ni_{1.1}MnAl_2$ shows the coercive field and remanence lower than FeCoNi.

From previous work [19, 20], the peaks observed in Figure 4a, along the hard axis hysteresis loop, are often measured for hysteresis loops taken on MOKE magnetometers, when the ferromagnetic sample has a strong anisotropy and obeys the Stoner-Wohlfarth model. This is because the Stoner-Wohlfarth model has two different energies associated with the ascending and descending magnetisation curves as a function of magnetic field. It has been found that when the magnetisation hysteresis loop is measured close to the hard axis, then peaks can be observed within the measured loops due to the crossing between these hysteresis branches. This effect has been observed for samples measured on a range of magnetometers including vibrating sample magnetometers (VSMs) and MOKE magnetometers. Thus the peaks occur due to the measurement taking place close to the hard axis of the sample, and crossing of hysteresis branches occurring.

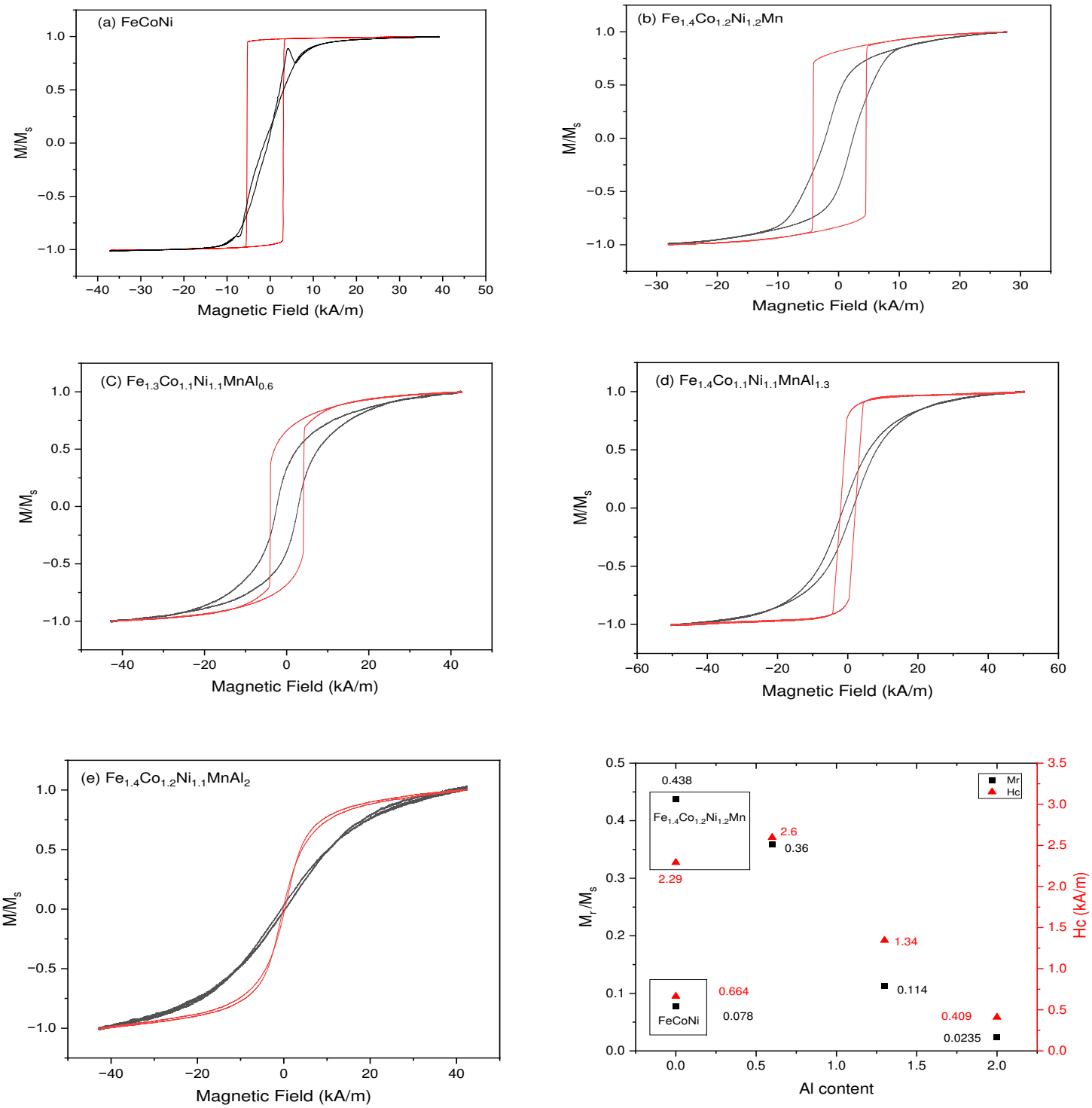


Figure 4. Shows the easy axis (read) and hard axis (black) hysteresis loop for all the alloys, as shown in (a), (b), (c), (d) and (e). (f) show the hysteresis loop, coercivity, and remanence for all the FeCoNiMnAl films as a function of Al composition.

There are three methods to identify the uniaxial anisotropy strength [21]. The first one is by calculating the anisotropy constant (K) by using the following equation.

$$K = \frac{H_k M_s \mu_0}{2} \quad \text{Equation 1}$$

$K$ represents the anisotropy constant, $H_k$ denotes the anisotropy field, $M_s$ is the saturation magnetisation, and $\mu_0$ is the permeability of free space.

The second method for calculating the strength of uniaxial anisotropy involves fitting the following equation to $M/M_s$ as a function of angle data. [22].

$$\frac{M_r}{M_s} = D|cos\ (\theta - \theta_0)| + C \quad \text{Equation 2}$$

$D$ denotes the magnitude of uniaxial anisotropy, $\theta$ represents the angle between the easy axis and the applied field, $\theta_0$ indicates the angle between the easy axis and the film's edge, and $C$ signifies the minimum recorded $\frac{M_r}{M_s}$. For an isotropic film, $D \approx 0$, as $\frac{M_r}{M_s}$ remains constant, for $D < 0.5$, the film' anisotropy exhibits weak uniaxial characteristics, while for $D > 0.5$, the anisotropy becomes strongly uniaxial.

The third method is a simpler methodology to the second method, where it takes the average of the remanence magnetisation of the hysteresis loop along the hard axis. This indicates whether the anisotropy is weak, strong or even isotropic, as the number, represented by M is between 0 and 1. It is a useful first calculation before the more complex second method.

Figure 5 shows the magnitude of uniaxial anisotropy (($D$) and (M)) and the anisotropy constant ($K$), which were calculated using the three methods given above. The magnitude of the uniaxial anisotropy was determined by both the second and third methods, yielding very similar results. The FeCoNi sample exhibits the highest values for both the magnitude of uniaxial anisotropy and the anisotropy constant, approximately 0.9 and 23 kJ/m³, respectively. This indicates a strong uniaxial anisotropy, as $D$ and M are close to the maximum value of 1, and $K$ is the highest compared to the other films.

When Mn is added to form $Fe_{1.4}Co_{1.2}Ni_{1.2}Mn$, the $D$ and M values drop below 0.5, indicating weak uniaxial anisotropy, which is correlated with a decrease in $K$. The sample with the highest percentage of aluminium ($Fe_{1.4}Co_{1.2}Ni_{1.1}MnAl_2$) shows almost isotropic anisotropy, as evidenced by $D$ and $M$ values close to 0 and the lowest $K$ value. Table 2 presents a comparison between the samples from this study and those from other works, highlighting the effect of elemental additions on the crystal structure and magnetic properties of FeCoNi alloys. The data indicates that the crystal structure of FeCoNi transitions from FCC to BCC with the incorporation of elements such as Al and Mn, as predicted from the VEC. Additionally, the saturation magnetisation and coercivity exhibit significant variations depending on the compositional changes. The saturation magnetization measured in the films is less than those measured in bulk, which may be due to the morphology of the films being amorphous/nanocrystalline, which tends to have a smaller magnetization than a fully polycrystalline film or bulk sample. Further the coercive field within the films is larger than those of the bulk, suggesting that although the films are amorphous/nanocrystalline, which normally would give a small coercive field, there are pinning sites within the films, such as non-magnetic inclusions, that are causing the domain walls within the films to pin, and therefore increase the measured coercive field.

Table 2 Comparison of magnetic properties and crystal structures between this work and previous studies. The saturation magnetization for the films from this paper were measured in kA/m, but converted to Am/kg by calculating the theoretical density of the films.

| Sample | Form | Phase | Ms ($Am^2/kg$) | Hc (kA/m) | Reference |
|---|---|---|---|---|---|
| FeCoNi | Bulk | FCC | 151.3 | 0.12 | [23] |
| FeCoNiAl | Bulk | BCC | 101.8 | 0.22 | [23] |
| $FeCoNiAl_{0.5}$ | Bulk | FCC+BCC | 105) | 0.36 | [23] |
| FeCoNiAlMn | Bulk | FCC+BCC | 94 | 0.4 | [24] |
| $FeCoNi(AlMn)_{0.1}$ | Bulk | FCC | 151.7 | 0.13 | [25] |
| FeCoNi | Thin film | FCC | 120 (1024 (kA/m)) | 0.67 | This work |
| $Fe_{1.4}Co_{1.1}Ni_{1.1}MnAl_{1.3}$ | Thin film | BCC | 64 (470 (kA/m)) | 1.34 | This work |

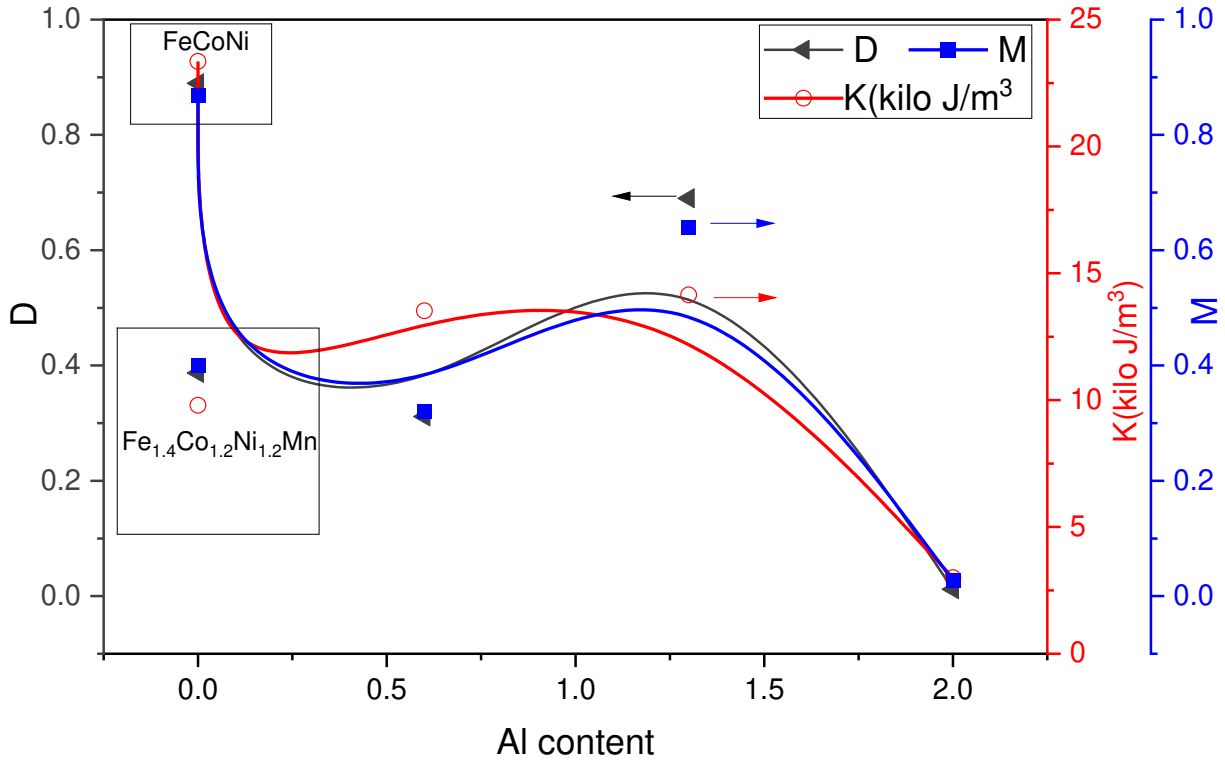


Figure 5. Uniaxial anisotropy strength ((*D*) and (M)) and the Anisotropy constant (*K*) as a function of Al contribution. The solid lines are a guide for the eye.

Figure 6 shows the anisotropy field ($H_k$) for the films measured along the hard axis. The $Fe_{1.2}Co_{1.2}Ni_{1.4}Mn$ film exhibits the lowest $H_k$ value, indicating it is easier to rotate its magnetisation from the hard axis to the easy axis, which is expected given its weak uniaxial anisotropy. Moreover, the low value for the $H_k$ for this film will also be due to the film having an amorphous structure (as shown in figure 3), which means it has no magnetocrystalline anisotropy contribution. In contrast, the $Fe_{1.4}Co_{1.1}Ni_{1.1}MnAl_{1.3}$ film has the highest $H_k$ value, indicating strong uniaxial anisotropy.

However, the $Fe_{1.4}Co_{1.2}Ni_{1.1}MnAl_2$ film exhibits the weakest uniaxial anisotropy and has an $H_k$ value, which is roughly similar to FeCoNi that has very strong uniaxial anisotropy. Figure 6 also displays the saturation magnetization ($M_s$) for the same set of films. FeCoNi shows the highest *Ms* value, which is comparable to the saturation magnetisation measured for bulk FeCoNi samples in the literature [4]. As expected the saturation magnetisation decreases as the paramagnetic elements are added to the films. Interestingly, when Mn and Al (0.6, 1.3) are added, the saturation magnetization remains relatively constant, likely due to the formation of the BCC phase, which has been shown to have a higher magnetization than the FCC phase [15]. However, for the $Fe_{1.4}Co_{1.2}Ni_{1.1}MnAl_2$ film, where the paramagnetic element concentration is relatively high, $M_s$ experiences a significant drop.

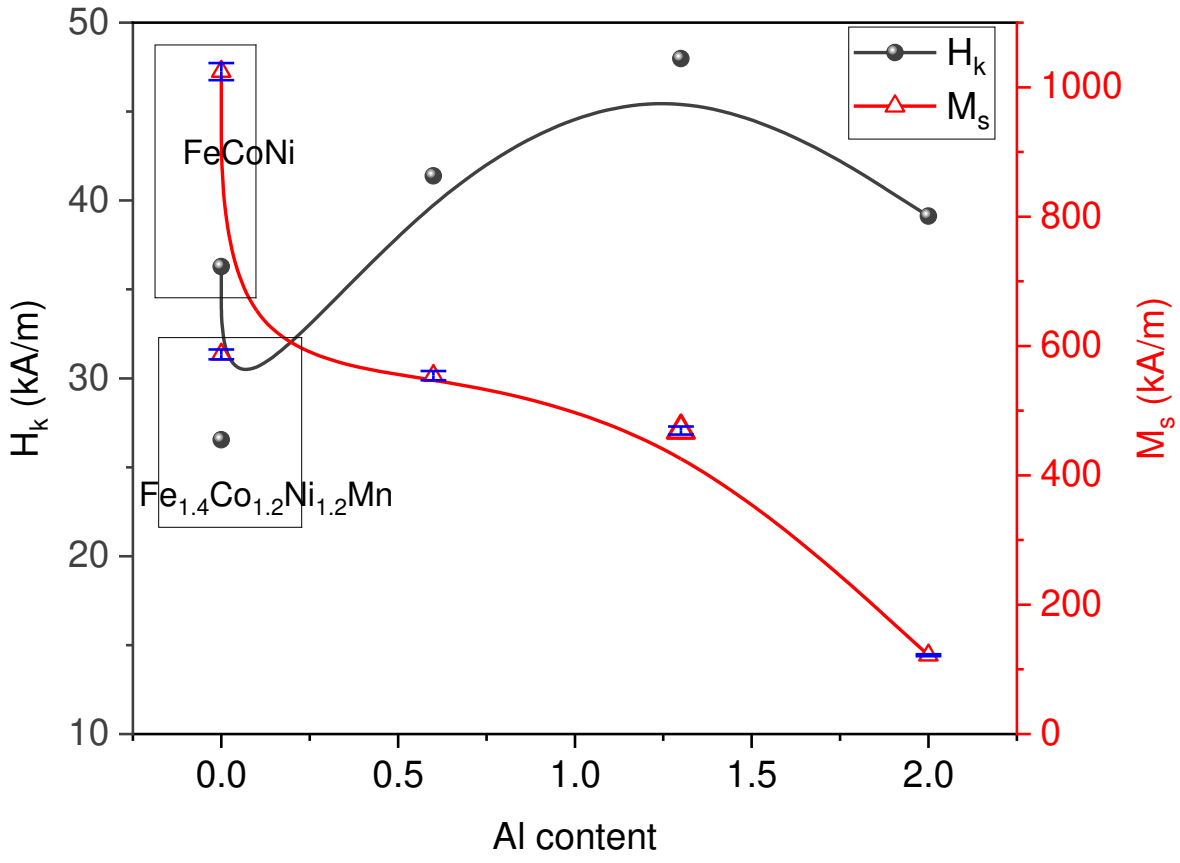


Figure 6. Anisotropy field ($H_k$) and saturation magnetisation ($M_s$) of all the films as a function of Al contribution. The solid lines are a guide for the eye.

### *C. Electrical properties*

Figure 7 illustrates the electrical resistivity ($\rho$) of the film set, which is a critical parameter for soft magnetic materials when used in applications, as it influences the energy dissipation and eddy currents within the film. Electrical resistivity is an inherent feature affected by the composition and the mobility of electrons within the material. The resistivity was measured by first determining the sheet resistance (*Rs*) using Equation 3, then calculating the resistivity from Equation 4[26].

$$Rs = \frac{V}{I} * CF \ (\Omega \ per \ square) \qquad \text{Equation 3}$$

$$\rho = Rs * t \ (\Omega \ m) \qquad \text{Equation 4}$$

where *Rs* is the sheet resistance, $\frac{V}{I}$ represents the electrical resistance of the film, *CF* is the correction factor, $\rho$ denotes the electrical resistivity of the film, and *t* is the thickness of the film.

The resistivity shows a noticeable increase as the Al content increases, which is expected because Al has a larger atomic size due to a greater atomic radius compared to other elements in the film composition. This larger atomic size results in increased electron scattering. Similar observations were reported by Akbari et al. when they added MnAl to FeCoNi and prepared the samples using vacuum arc melting [26].

Taking account of both the magnetic and resistivity results, the $Fe_{1.4}Co_{1.1}Ni_{1.1}MnAl_{1.3}$ film has a decrease of about third in saturation magnetisation compared to the $Fe_{20}Ni_{80}$ film, but a large increase in resistivity of over two orders of magnitude, this reduces eddy currents, which is crucial for applications involving high-frequency magnetic fields.

Another reason to investigate new soft magnetic materials, is the cost of the some of the magnetic elements: Co (24.30 \$/kg) and Ni (16.21 \$/kg) are more expensive than Fe (0.105 \$/kg), while elements such as Mn (2.11 \$/kg) and Al (2.62 \$/kg) are relatively cheap [27]. Therefore, the addition of Mn and Al to FeCoNi will reduce the overall cost of the raw materials. For example, the FeCoNi film cost is 13.16 \$/kg, while for the $Fe_{1.4}Co_{1.1}Ni_{1.1}MnAl_{1.3}$ film, the cost is 9.43 \$/kg, which is a 28 % decrease and for the $Fe_{1.3}Co_{1.1}Ni_{1.1}MnAl_{0.6}$ film, the cost is 10.29 \$/kg, which is a 22 % decrease [27].

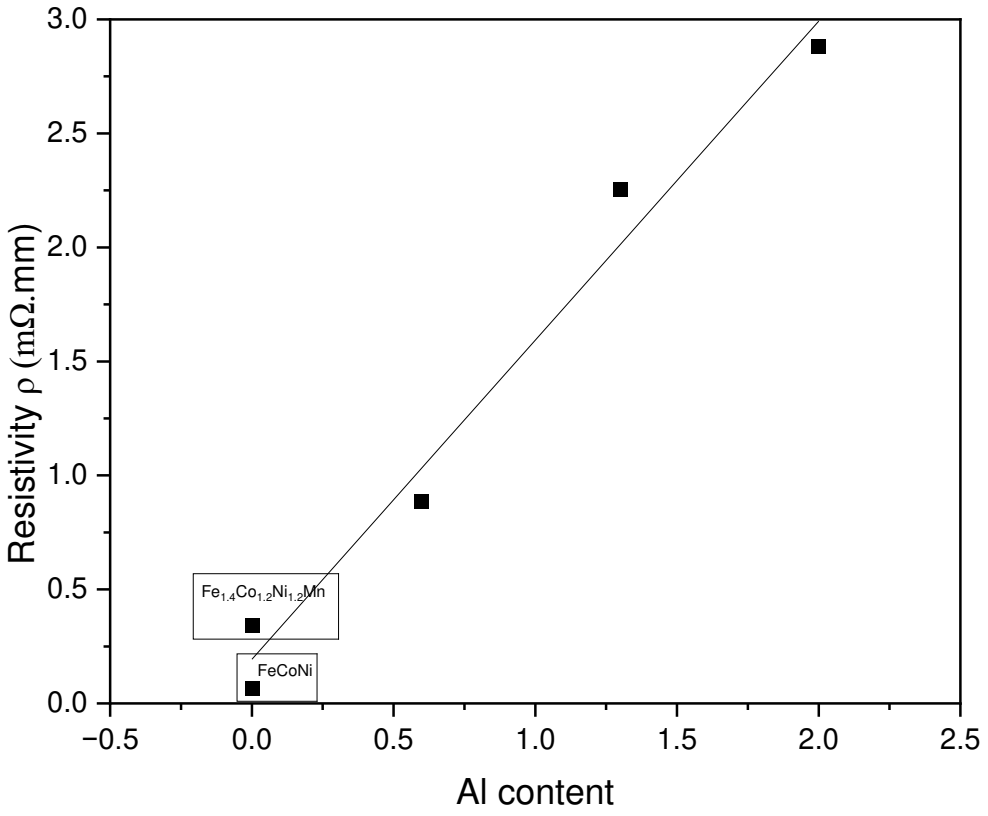


Figure 7. Electrical resistivity of all the films as a function of Al composition. The solid line is a linear fit to the data.

## IV. Conclusion

DC sputtering was successfully used to produce a set of $FeCoNiMnAl_x$ films with a thickness of 100 nm. The FeCoNi film exhibited an FCC crystalline structure, while the $Fe_{1.4}Co_{1.2}Ni_{1.2}Mn$ film was amorphous. The addition of Al with concentrations of 0.6, 1.3, and 2 to the FeCoNiMn films indued a BCC structure. The $Fe_{1.4}Co_{1.2}Ni_{1.1}MnAl_2$ film had the highest content of paramagnetic elements (Al and Mn) and showed the lowest values for coercivity and remanence. The FeCoNi film exhibited uniaxial anisotropy, whereas the $Fe_{1.4}Co_{1.2}Ni_{1.1}MnAl_2$ film was isotropic. The highest saturation magnetisation was measured in the FeCoNi film but decreased as the concentration of paramagnetic elements increased. The decrease in the saturation magnetization was non-linear, due to the formation of the BCC phase within the films. The electrical resistivity reached a maximum value of 2.9 mΩ·mm for the $Fe_{1.4}Co_{1.2}Ni_{1.1}MnAl_2$ film, compared to 0.06 mΩ·mm for the FeCoNi film. Taking account of the decrease in saturation magnetisation, with the increase in electrical resistivity, the $Fe_{1.4}Co_{1.1}Ni_{1.1}MnAl_{1.3}$ film is a promising candidate as a new soft magnetic material.

**Funding sources**

This research was funded by Saudi Arabia Government and the Henry Royce Institute for Advanced Materials, funded through EPSRC grants EP/R00661X/1, EP/S019367/1, EP/P02470X/1 and EP/P025285/1, for the SQUID access at The University of Sheffield.

**Author contributions: CRediT**

D.M. Alsebaie: Data curation, Formal analysis, Investigation, Writing – original draft.

N. A. Morley: Conceptualization, Project administration, Resources, Supervision, Writing – original draft, Writing – review and editing.

Reference

1. Abbas, Q.A., et al., *Influence of annealing temperature on the structural and magnetic properties of FeGaSiB thin films*. Thin solid films, 2020. **701**: p. 137955.
2. Abbas, Q.A. and N.A. Morley, *Fabrication and characterization of magnetostrictive amorphous FeGaSiB thin films*. Journal of magnetism and magnetic materials, 2017. **439**: p. 353-357.
3. Ali, M. and F. Ahmad, *A review of processing techniques for Fe-Ni soft magnetic materials*. Materials and Manufacturing Processes, 2019. **34**(14): p. 1580-1604.
4. Kunwar, S., J. Arout Chelvane, and M. Manivel Raja, *Structural, magnetic and Magnetic-Microstructural properties of sputtered FeCoNi thin films*. Journal of Magnetism and Magnetic Materials, 2023. **572**: p. 170597.
5. Bardos, D., *Mean magnetic moments in bcc Fe–Co alloys*. Journal of Applied Physics, 1969. **40**(3): p. 1371-1372.
6. Sundar, R. and S. Deevi, *Soft magnetic FeCo alloys: alloy development, processing, and properties*. International materials reviews, 2005. **50**(3): p. 157-192.
7. Sourmail, T., *Near equiatomic FeCo alloys: Constitution, mechanical and magnetic properties*. Progress in materials science, 2005. **50**(7): p. 816-880.
8. Xiaomin, L., P. Evans, and G. Zangari, *Electrodeposited Co-Fe and Co-Fe-Ni alloy films for magnetic recording write heads*. IEEE transactions on magnetics, 2000. **36**(5): p. 3479-3481.

9. Kockar, H., et al., *Differences observed in properties of ternary NiCoFe films electrodeposited at low and high pH*. Journal of Materials Science: Materials in Electronics, 2013. **24**(6): p. 1961-1965.
10. *Fundamentals of materials science and engineering; an interactive e-text. (CD-ROM included)*, in *Scitech Book News*. 2001, Copyright Clearance Center: Portland.
11. Morley, N.A., et al., *Magnetic properties of the complex concentrated alloy system CoFeNi0.5Cr0.5Alx*. 2020.
12. Harris, J., et al., *Investigation into the magnetic properties of CoFeNiCryCux alloys*. Journal of Physics D: Applied Physics, 2021. **54**(39): p. 395003.
13. Quintana-Nedelcos, A., et al., *On the structural, microstructural and magnetic properties evolution of Ni0.5FeCoAlCrx alloys*. Materials Letters, 2022. **311**: p. 131542.
14. Bazioti, C., et al., *Probing the structural evolution and its impact on magnetic properties of FeCoNi (AlMn) x high-entropy alloy at the nanoscale*. Journal of Alloys and Compounds, 2022. **910**: p. 164724.
15. Rowan-Robinson, R.M., Z. Leong, and N.A. Morley, *CoFeMn0.5Al0.25: A high magnetisation CoFe based soft alloy with reduced Co content*. Materials chemistry and physics, 2023. **299**: p. 127518.
16. Li, W., L. Ping, and P.K. and Liaw, *Microstructures and properties of high-entropy alloy films and coatings: a review*. Materials Research Letters, 2018. **6**(4): p. 199-229.
17. Li, P., A. Wang, and C.T. Liu, *Composition dependence of structure, physical and mechanical properties of FeCoNi(MnAl)x high entropy alloys*. Intermetallics, 2017. **87**: p. 21-26.
18. Zhang, Y., et al., *Compositional design of soft magnetic high entropy alloys by minimizing magnetostriction coefficient in (Fe0.3Co0.5Ni0.2)100-x(Al1/3Si2/3)x system*. Metals (Basel ), 2019. **9**(3): p. 382.
19. Morley, N.A., et al., *MOKE hysteresis loop method of determining the anisotropy constants of ferromagnetic thin films: fe on GaAs(100) with overlayers of Au and Cr*. Journal of Magnetism and Magnetic Materials, 2006. **300**(2): p. 436-444.
20. Mathews, S.A., A.C. Ehrlich, and N.A. Charipar, *Hysteresis branch crossing and the Stoner–Wohlfarth model*. Scientific Reports, 2020. **10**(1): p. 15141.
21. Abbas, Q.A., et al., *Influence of Ga evaporation rate on the magnetic properties of Amorphous FeGaSiB thin films*. Journal of magnetism and magnetic materials, 2020. **498**: p. 166160.
22. Miskevich, E., et al., *Artificial multiferroic structures using soft magnetostrictive bilayers on Pb(Mg1/3Nb2/3)-PbTiO3*. 2018.
23. Zuo, T.T., et al., *Effects of Al and Si addition on the structure and properties of CoFeNi equal atomic ratio alloy*. Journal of Magnetism and Magnetic Materials, 2014. **371**: p. 60-68.
24. Hariharan, V.S., et al., *Effect of Al addition and homogenization treatment on the magnetic properties of CoFeMnNi high-entropy alloy*. Journal of Materials Science, 2020. **55**(36): p. 17204-17217.

25. Li, Z., et al., *Tuning phase constitution and magnetic properties by composition in FeCoNiAlMn high-entropy alloys*. Journal of Alloys and Compounds, 2020. **845**: p. 156204.
26. Akbari, A., et al., *Effects of annealing and cold rolling on microstructural features, magnetic properties, tensile behavior and electrical resistance of FeCoNi(MnAl)x high entropy alloys*. Intermetallics, 2024. **175**: p. 108521.
27. *Daily Metal Prices*. 2024 8/11/2024]; Available from: https://www.dailymetalprice.com/.